



Effects of extremely low-frequency magnetic fields on human MDA-MB-231 breast cancer cells: proteomic characterization

Raffaella Lazzarini^a, Maria Eléxpuru-Zabaleta^b, Francesco Piva^c, Matteo Giulietti^c, Gianluca Fulgenzi^d, Maria Fiorella Tartaglione^a, Laura Zingaretti^e, Adriano Tagliabracci^f, Matteo Valentino^a, Lory Santarelli^{a,*}, Massimo Bracci^{a,*}

^a Occupational Medicine, Department of Clinical and Molecular Sciences, Polytechnic University of Marche, 60126 Ancona, Italy

^b Research Group on Foods, Nutritional Biochemistry and Health, Universidad Europea del Atlántico, 39011 Santander, Spain

^c Department of Specialistic Clinical and Odontostomatological Sciences, Polytechnic University of Marche, 60131 Ancona, Italy

^d Experimental Pathology, Department of Clinical and Molecular Sciences, Polytechnic University of Marche, 60126 Ancona, Italy

^e Occupational Medicine Unit, Marche University Hospital, 60126 Ancona, Italy

^f Department of Excellence of Biomedical Sciences and Public Health, Polytechnic University of Marche, Ancona, Italy

ARTICLE INFO

Edited by - Yong Liang

Keywords:

Extremely low-frequency magnetic fields (ELF-MF)
Breast cancer
Proteome profiling
Oxidative stress
Cell adhesion
Cellular reprogramming

ABSTRACT

Extremely low-frequency electromagnetic fields (ELF-MF) can modify the cell viability and regulatory processes of some cell types, including breast cancer cells. Breast cancer is a multifactorial disease where a role for ELF-MF cannot be excluded. ELF-MF may influence the biological properties of breast cells through molecular mechanisms and signaling pathways that are still unclear. This study analyzed the changes in the cell viability, cellular morphology, oxidative stress response and alteration of proteomic profile in breast cancer cells (MDA-MB-231) exposed to ELF-MF (50 Hz, 1 mT for 4 h). Non-tumorigenic human breast cells (MCF-10A) were used as control cells. Exposed MDA-MB-231 breast cancer cells increased their viability and live cell number and showed a higher density and length of filopodia compared with the unexposed cells. In addition, ELF-MF induced an increase of the mitochondrial ROS levels and an alteration of mitochondrial morphology. Proteomic data analysis showed that ELF-MF altered the expression of 328 proteins in MDA-MB-231 cells and of 242 proteins in MCF-10A cells. Gene Ontology term enrichment analysis demonstrated that in both cell lines ELF-MF exposure up-regulated the genes enriched in “focal adhesion” and “mitochondrion”. The ELF-MF exposure decreased the adhesive properties of MDA-MB-231 cells and increased the migration and invasion cell abilities. At the same time, proteomic analysis, confirmed by Real Time PCR, revealed that transcription factors associated with cellular reprogramming were upregulated in MDA-MB-231 cells and downregulated in MCF-10A cells after ELF-MF exposure. MDA-MB-231 breast cancer cells exposed to 1 mT 50 Hz ELF-MF showed modifications in proteomic profile together with changes in cell viability, cellular morphology, oxidative stress response, adhesion, migration and invasion cell abilities. The main signaling pathways involved were relative to focal adhesion, mitochondrion and cellular reprogramming.

1. Introduction

In recent years, biomedical researchers increasingly contribute to the knowledge of the interactions between extremely low-frequency magnetic fields (ELF-MF) and the biology of human cells (Koziorowska et al., 2017; Maes and Verschaeve, 2016; Makinistian et al., 2019). The ever

increasing use of electricity is generating a widespread presence of 50–60 Hz ELF-MF (Tomitsch and Dechant, 2015) which raise concern for their potential health risks (Bernard et al., 2008). Epidemiological studies have demonstrated an association of ELF-MF exposure with cancer, cardiovascular and neurological diseases in adults (Carpenter, 2019; Koeman et al., 2013; Mattsson and Simkó, 2012; Zhang et al.,

* Corresponding authors.

E-mail addresses: r.lazzarini@staff.univpm.it (R. Lazzarini), maria.elpuru@uneatlantico.es (M. Eléxpuru-Zabaleta), f.piva@staff.univpm.it (F. Piva), [m.giulietti@staff.univpm.it](mailto:giulietti@staff.univpm.it) (M. Giulietti), g.fulgenzi@staff.univpm.it (G. Fulgenzi), m.f.tartaglione@pm.univpm.it (M.F. Tartaglione), laura.zingaretti@ospedaliriuniti.marche.it (L. Zingaretti), a.tagliabracci@staff.univpm.it (A. Tagliabracci), m.valentino@staff.univpm.it (M. Valentino), l.santarelli@staff.univpm.it (L. Santarelli), m.bracci@staff.univpm.it (M. Bracci).

<https://doi.org/10.1016/j.ecoenv.2023.114650>

Received 20 July 2022; Received in revised form 29 January 2023; Accepted 11 February 2023

Available online 16 February 2023

0147-6513/© 2023 The Authors. Published by Elsevier Inc. This is an open access article under the CC BY-NC-ND license (<http://creativecommons.org/licenses/by-nc-nd/4.0/>).

2016). In 1979, the earliest epidemiological analysis reported an association between ELF-MF exposure and the increased risk of childhood leukemia (Wertheimer and Leeper, 1979). In 2002, ELF-MF were classified by the World Health Organization's International Agency for Research on Cancer (IARC) as possible carcinogens for humans (category 2B) (IARC, 2002). Successive epidemiological surveys and in vivo and in vitro studies have evaluated the carcinogenicity of ELF-MF exposure (Bernard et al., 2008; Núñez-Enríquez et al., 2020). ELF-MF do not have a direct role in carcinogenesis, but they contribute altering cellular homeostasis. (Carpenter, 2019; Lee et al., 2012; Maffei, 2022). To date, ELF-MF have been shown to alter some cell functions such as redox homeostasis, proliferation, differentiation, and adhesion (Baek et al., 2014; Du et al., 2014; Nezamtaberi et al., 2022; Ross, 2017; Sulpizio et al., 2011; Wolf et al., 2005), but the molecular mechanism regulating the pathogenic effects remains elusive.

Breast cancer development and progression are multifactorial processes in which cellular and molecular events promote unrestrained cell proliferation and an alteration of cell functions and cell morphology (Feng et al., 2018). Cell differentiation, migration, and adhesion have a crucial role in physiological development and disease-related processes, including carcinogenesis. The reprogramming of normal breast cells into cancer cells and the maintenance of the tumor phenotype have been associated with the epigenetic dysregulation and overexpression of pluripotency factors (Giorgi and Del Re, 2021; Taurin and Alkhalifa, 2020). Notably, pluripotency in terminally differentiated breast cancer cells can be reestablished through the expression of transcription factors to induce the transition to breast cancer stem cells (Corominas-Faja et al., 2013; Lieblein et al., 2008; Tiwari et al., 2013). Focal adhesion, which plays a pivotal role in cancer cell mobility and invasiveness (Luo and Guan, 2010), is controlled by a multiprotein complex that links the actin cytoskeleton to the extracellular matrix. Breast cancer cells have altered focal adhesion dynamics (Chan et al., 2009; Wu et al., 2020). ELF-MF exposure may enhance and/or activate molecular pathways involved in breast carcinogenesis and cancer progression (Carpenter, 2019; Masoudi-Khoram and Abdolmaleki, 2022).

In this work, we used proteome profiling to identify homology and/or differences in protein expression patterns in MDA-MB-231 triple-negative human breast cancer cells and MCF-10A normal human breast cells exposed to ELF-MF (50 Hz, 1 mT for 4 h). Among the proteins showing differential expression in the two cell lines, Gene Ontology (GO) term enrichment analysis demonstrated key factors belonging to "focal adhesion" and "mitochondrion". In addition, the breast cancer cell line showed up-regulation of reprogramming factors.

2. Materials and methods

2.1. Cell lines

MDA-MB-231 triple-negative breast cancer cells and MCF-10A normal human breast epithelial cells (non-tumorigenic) were obtained from the Experimental Zooprophyllaxis Institute of Lombardia and Emilia Romagna (Brescia, Italy). MDA-MB-231 breast cancer cells were cultured in Dulbecco's Modified Eagle's Medium (DMEM, Euroclone, Pero, Italy), supplemented with 10% fetal bovine serum (FBS, Euroclone); and 2 mM L-glutamine (Euroclone) and penicillin/streptomycin (1:100, Euroclone). MCF-10A cells were maintained in DMEM/F12 medium with L-glutamine (Euroclone) and 5% horse serum (Thermo Fisher Scientific, Milano, Italy), 20 ng/ml epidermal growth factor, 0.5 µg/ml hydrocortisone, 100 ng/ml cholera toxin, 10 µg/ml insulin (all reagents were purchased from Merck KGaA Darmstadt, Germany), and penicillin/streptomycin (1:100) (Thermo Fisher Scientific). Both cell lines were cultured at a 37.0 °C in a 5% CO₂, 90% humidified incubator and the medium was changed every 3 days.

2.2. Electromagnetic field exposure

A square Helmholtz coil was used to generate 50 Hz ELF-MF, using a magnetic flux density of 1 mT. The exposure system was self-designed and built for use inside a cell incubator. Considering the thermal insulation of the incubator, the coil was designed to prevent dissipation of the electric power exceeding 8 W. The dimensions (inner coil sides, 34 × 34 cm) and the distances between the two solenoids (19.5 cm) were taken from the simulations and tests reported in literature (Abbott, 2015). The 50 Hz 1 mT ELF-MF produced by the generator in the incubator was verified with a professional ELF-MF analyzer (EFA-300, Wandel & Goltermann, Germany). After seeding, MDA-MB-231 and MCF-10A cells were placed between the coils in the incubator (37.0 ± 0.1 °C and 5% CO₂). The unexposed control cells were placed in another incubator and were not exposed to ELF-MF (50 Hz ELF-MF generated by the incubator was 0.792 µT). After 4 h, the exposed cells were placed into the same incubator as the unexposed cells. All cell groups were analyzed 4 days from seeding. To exclude any changes in microenvironmental temperature, the temperature was constantly measured during the experiment with a ThermoChron iButton DS1922L analyzer (Maxim Integrated Products, San Jose, CA, USA).

2.3. Trypan blue assay

For the trypan blue assay, MDA-MB-231 and MCF-10A cells were plated in 6-well plates (Costar, Corning Inc., Corning, NY, USA) at a seeding density of 8×10^4 cells/well, and were exposed to 50 Hz, 1 mT ELF-MF. The live/dead assay was performed after 96 h of exposure using 0.4% trypan blue (1:1; Thermo Fisher Scientific). The number of live and dead cells was obtained using a Countess Automated Cell Counter (Thermo Fisher Scientific). Cells were observed prior to the trypsin treatment and photographed under an inverted microscope (Leitz Fluovert; Leica Microsystems Inc., Germany) equipped with a digital camera (Canon EOS M50; Canon Inc., Japan). The experiment was performed in triplicate and repeated three times.

2.4. Cell viability assay

Cell viability was tested using cell titer-blue cell viability assay, following the manufacturer's recommendations (Promega, Milano, Italy). Briefly, 1×10^3 MDA-MB-231 and 1×10^3 MCF-10A cells were seeded in 96-well plates (Costar), exposed to 50 Hz, 1 mT ELF-MF for 4 h, and subsequently placed in an incubator (37 °C, 5% CO₂ humidified incubator) for 96 h, unexposed cells were used as a control. 20 µl cell of titer-blue was added to each well after 4 h of incubation and fluorescence intensity was analyzed using a microplate ELISA reader (Sunrise; Tecan Group Ltd., Männedorf, Switzerland) with a 535/25 Ex and 590/20 Em filter set. The experiment was performed in triplicate and repeated three times.

2.5. Phalloidin staining

For phalloidin staining, MDA-MB-231 and MCF-10A cells were seeded on chamber slides and exposed to 50 Hz, 1 mT ELF-MF for 4 h. Then, exposed and control cells were cultured for 96 h. Subsequently, cells were fixed using 4% paraformaldehyde solution in PBS (phosphate buffered saline) for 30 min and permeabilized with 0.1% Triton X-100 in PBS for 20 min at room temperature. TRITC-labeled phalloidin (Merck KGaA) was used to stain cells, according to the manufacturer's protocol. Vectashield mounting medium was added to slides (Vector Laboratories, Burlingame, CA, USA) and the cells were analyzed under a fluorescence microscope (Zeiss AX10 Imager, Carl Zeiss Inc., Germany) equipped with a FL-20 low noise CMOS camera (Axiom Optics Inc., Somerville, MA, USA). The length and number of filopodia and filopodia-like structures from microscopy images of phalloidin stained cells were detected and measured using the Single image FiloQuant plugin for the

ImageJ software (ver. 2.1.0/1.53c) (Jacquemet et al., 2019, 2017). Filopodia density was defined as a ratio of the number of detected filopodia to the number of cells in each image. Each assay was performed in triplicate and repeated three times.

2.6. Apoptosis assay

Necrosis, early and late apoptotic rate were evaluated using the Apoptosis detection kit (eBioscience, Thermo Fisher Scientific), according to the supplier's instructions. Briefly, after 96 h from seeding, unexposed (CTRL) and ELF-MF exposed cells were harvested and then fixed and dual stained with Annexin V and propidium iodide. About 20,000 cells were analyzed for each sample using a FACSCalibur flow cytometer (BD Biosciences, Allschwil, Switzerland) equipped with Cell Quest software set on a logarithmic scale (BD Biosciences, San Jose, CA, USA). Data analysis was performed using FlowJo 10.7.2. software (BD Biosciences). Each assay was performed in triplicate and repeated three times.

2.7. Transmission electron microscopy (TEM)

MDA-MB-231 and MCF-10A breast cells were plated on ACLAR film (Ted Pella, CA, USA) at seeding density of $1 \times 10^5/\text{cm}^2$. Unexposed and ELF-MF exposed cells were fixed in glutaraldehyde 2.5% in phosphate buffer pH 7.4 for 1 h at room temperature and subsequently overnight at 4 °C. Cells were washed in buffer and post-fixed in osmium tetroxide 0.5% for one hour. All samples were dehydrated with acetone series and flat embedded in Luft epoxy resin using a polystyrene capsule. Once the resin hardened, ACLAR was peeled off and ultrathin sections (50 nm) were cut then stained using lead citrate, then imaged at 80 kV in a Philips CM10 electron microscope (FEI, Hillsboro, Oregon, USA). The experiment was performed in triplicate and repeated three times.

2.8. ROS measurement

Cells, at a density of 5×10^3 cells/well, were plated in 96-well black plate (Corning, Glendale, Arizona, USA) and exposed to ELF-MF for 4 h. After 96 h, exposed (ELF-MF) and unexposed cells (CTRL) were stained with 2.5 μM of MitoSOX red (Thermo Fisher Scientific) at 37 °C for 20 min to measure mitochondrial ROS levels. After 3X washing with HBSS (Thermo Fisher Scientific), fluorescence at excitation/emission wavelengths of $535 \pm 25/590 \pm 20$ nm was measured using a microplate reader (Sunrise; Tecan Group Ltd). All measurements were normalized for the number of cells, quantified using Hoechst 33342 DNA-binding dye (Thermo Fisher Scientific) and measuring fluorescence at excitation/emission wavelengths of $340 \pm 35/465 \pm 35$ nm. Antimycin A (Merck KGaA) was used as a positive control at 25 μM (final concentration) for 30 min at 37.0 ± 0.1 °C and 5% CO₂. The experiment was performed in triplicate and repeated three times.

2.9. Protein extraction, protein digestion and peptide preparation for Mass Spectrometry analysis

For protein extraction, MDA-MB-231 and MCF-10A cells were seeded in 6 wells (2×10^5 cells/well) and exposed to 50 Hz, 1 mT ELF-MF for 4 h. After 96 h of incubation, cells were washed with 1x PBS and Urea buffer 8 M-Tris 100 mM HCL (150 μl /well in a 6-well plate) was used to scrape them. Lysates were incubated 30 min on ice vortexing every 10 min. Samples were centrifuged (Eppendorf® Microcentrifuge 5415, Eppendorf, Hamburg, Germany; Merck KGaA) at 16,000 x g for 20 min at 4 °C. Protein concentrations were measured using a Bradford assay (Merck KGaA). About 25 μg of protein per sample was resuspended in 8 M Urea 10 mM Tris-HCl buffer. The samples were reduced by TCEP and then alkylated using chloroacetamide (Kulak et al., 2014). Peptides were digested by Lys-C and trypsin, desalted in a C18 Stage Tip (Thermo Fisher Scientific) and resuspended in 20 μl Solvent A (2% acetonitrile,

0.1% formic acid).

2.9.1. Mass spectrometry analysis and proteins quantification

Label-free quantification method achieves high-proteome coverage and provides high dynamic range of quantification for large-scale proteome analysis despite it does not use a stable isotope for chemical binding and labeling of proteins. This is a robust and reliable method for relative quantification of proteins from a complex biological sample (Mittal et al., 2020). An LC-ESI-MS-MS quadrupole Orbitrap Q-Exactive HF mass spectrometer (Thermo Fisher Scientific) was used to analyze 5 μl of each sample as technical replicates. Peptides separation was achieved on a linear gradient from 95% solvent A to 30% solvent B (80% acetonitrile, 0.1% formic acid) over 210 min, from 30% to 60% Solvent B in 20 min and from 60% to 100% Solvent B in 2 min at a flow rate of 0.25 $\mu\text{l}/\text{min}$ on a UHPLC Easy-nLC 1000 apparatus (Thermo Fisher Scientific) connected to a 23-cm fused-silica emitter of 75 μm inner diameter (New Objective, Inc. Woburn, MA, USA), packed in-house with ReproSil-Pur C18-AQ 1.9 μm beads (Dr Maisch GmbH, Ammerbuch, Germany) using a high-pressure bomb loader (Proxeon, Odense, Denmark) (Rappsilber et al., 2003). For MS spectra (300–1650 Th) the resolution was 60,000 AGC target 3e6, and IT 20 ms. For HCD spectra, the resolution was 15,000 at m/z 200, AGC target 1e5, IT 80 ms, NCE 28% and isolation width 2.0 m/z . MaxQuant version 1.5.2.8 was used to process the raw data (Cox and Mann, 2008). The Andromeda search engine was used to identify peptides from the MS-MS spectra searched against the uniprot_cp_Homo Sapiens (98036 entries) (Cox et al., 2011). The mass deviation was set at 5 ppm for MS and at 20 ppm for MS-MS peaks. Peptide and protein false discovery rates (FDRs) were set at 0.01 and 6 amino acids was the minimal length for a peptide. Reverse hits and known contaminants were removed from the lists of proteins. Label-free analysis was carried out using the intensity values normalized across the entire dataset, a minimum ratio count of 2 and a 'match between runs' option.

The protein levels of the ELF-MF exposed and control samples of each cell line were analyzed using the Perseus software platform in the MaxQuant environment (<http://www.coxdocs.org>) with a P-value of 0.05 following the steps described by Tyanova et al. (Tyanova and Cox, 2018; Tyanova et al., 2016). Missing values were replaced by random numbers drawn from a normal distribution by the function 'imputation' (width 0.3, down shift 1.8, separately for each column). Hierarchical clustering was set with the following parameters: distance, Euclidean; linkage, average; number of clusters, 300, for both row and column tree dendrograms.

Additionally, the Linear Discriminant Analysis Effect Size tool (LEfSe; <https://huttenhower.sph.harvard.edu/lefse/>) was used to detect the significantly different relative abundances of proteins after ELF-MF exposure in each cell line. We used the default settings: $\alpha = 0.05$ and LDA score > 2 (Segata et al., 2011).

2.9.2. Bioinformatics analysis. Functional enrichment analyses

Each differentially expressed protein identified by the analysis was assigned to the respective human official NCBI Gene Symbol identifier. The gene symbols were then submitted to the WebGestalt (version 2019) (<http://webgestalt.org>) and Enrichr (<https://maayanlab.cloud/Enrichr/>) web tools. The two tools were used for gene list enrichment analysis to elucidate the underlying molecular mechanisms altered by ELF-MF. In particular, statistical enrichment of the GO term (sections "Biological Process", "Molecular Function", and "Cellular Component", release Jan. 2019 and Kyoto Encyclopedia of Genes and Genomes [KEGG, release 88.2, Nov. 2018]) pathway database was assessed by submitting the gene lists to WebGestalt. Enrichr was requested to identify enriched transcription factors (module "ENCODE and ChEA Consensus TFs from CHIP-X"). Up- and downregulated genes were submitted separately to the web tools: although all differentially expressed genes/proteins can be analyzed together, several recent studies have suggested that separate analysis of the lists of up- and downregulated

genes yields more accurate results (Hong et al., 2014; Razavi et al., 2017). Statistically significant terms were selected for further analysis if they reached an adjusted p-value < 0.05, according to the Benjamini-Hochberg correction for multiple hypothesis testing.

2.10. Adhesion assay

For the adhesion assay ELF-MF exposed and unexposed cells were trypsinized and the number of live cells was calculated using a Countess Automated Cell Counter (Thermo Fisher Scientific). The plates were rinsed and blocked with 10 mg/ml heat denatured BSA (Bovine Serum Albumine, Merck KGaA) for 30 min at room temperature. Cells were plated, at a density of 2×10^4 to each well, and incubated for 1 h at 37.0 °C in a 5% CO₂ incubator. Cells were washed with PBS and fixed with ice cold 70% ethanol at 4 °C for 10 min. The cell staining was performed using 0.2% crystal violet for 15 min. Cells were eluted with 10% acetic acid in an orbital shaker for 5 min at room temperature. Absorbance was measured at 570 nm using a microplate reader (Sunrise; Tecan Group Ltd). The experiment was performed in triplicate and repeated three times.

2.11. Transwell migration and invasion assays

Transwell chambers (96-well, 8 µm pore size, Corning Incorporated, Corning, NY, USA) were used to perform both cell migration and invasion assays. Normal breast cells and cancer cells exposed and unexposed to ELF-MF were treated with trypsin and live cells number were obtained by a Countess Automated Cell Counter (Thermo Fisher Scientific). For the migration and invasion assays 2×10^4 cells were seeded into the upper chamber of the Transwell, using serum free medium. Culture medium supplemented with 10% FBS (used as a chemoattractant), was added in the lower chamber. After 48 h, cotton swabs were used to remove non-migrated and non-invaded cells on the upper side of the membrane. Migrated and invaded cells were fixed with ice cold 70% ethanol at 4 °C for 10 min and stained with 0.2% crystal violet (Merck KGaA) for 15 min. Cells were counted in five selected fields using a Zeiss AX10 Imager microscope (Carl Zeiss Inc.). The results are reported as a mean cell number per membrane. For the invasion assay, 2×10^4 cells were seeded into GelTrex (Thermo Fisher Scientific) coated Transwell inserts. The time for the invasion assay was 48 h and cells were fixed, stained, and analyzed as described above. The experiments were performed in triplicate and repeated three times.

2.12. Total RNA extraction

To isolate total RNA, approximately 2.5×10^5 cells of each sample (MDA-MB-231 and MCF-10A cells exposed/not exposed to ELF-MF) were processed with RNeasy Mini Kit (Qiagen, GmbH, Hilden, Germany) following the manufacturer's protocol. RNA quantity and quality were measured using a NanoDrop One spectrophotometer (NanoDrop Technologies Inc., Wilmington, DE, USA). RNA was stored at -80 °C until use, and 500 ng of total RNA obtained from each sample was reverse-transcribed using the High-Capacity cDNA Reverse Transcription Kit (Thermo Fisher Scientific), according to the manufacturer's instructions.

2.13. Quantitative Real Time-PCR (qRT-PCR)

Quantitative real-time PCR (qRT-PCR) analysis was performed using a Master Cycle instrument (Eppendorf). Syber Select Master Mix (Thermo Fisher Scientific) and FluocycleII master Mix for probes (Euroclone) were used. Syber green real time PCR analysis was set up to analyze the expression levels of *KLF4* gene. *GAPDH* gene, commonly used as a reference gene expression level, was used for data normalization, the primer sequences are listed in Table 1. The amplification of Human *STAT3*, *BCLAF1*, *NR2C2*, *UBTF*, *USF1*, *CEBPD*, *ZMIM1*, *CHD1*

Table 1

Oligonucleotide sequences designed for target and reference gene.

Genes	Primer Forward (5'→3')	Primer Reverse (5'→3')
<i>KLF4</i>	CCCACACAGGTGAGAAACCT	ATGTGTAAAGGCGAGGTGGTC
<i>GAPDH</i> ¹	AGCCACATCGCTCAGACAC	GCCCAATACGACCAAAATCC

KLF4=Kruppel-like factor 4; *GAPDH*=Glyceraldehyde-3-Phosphate Dehydrogenase.

¹ Reference gene.

and *GAPDH* mRNA was performed using the TaqMan primer and probe set (Thermo Fisher Scientific). The experiments were performed in triplicate and repeated three times.

In each sample, the mRNA expression level of target genes was quantified with the $2^{-\Delta\Delta Ct}$ (fold change) method: $\Delta\Delta Ct = \Delta Ct (CTRL) - \Delta Ct (ELF-MF)$; a fold-change ≥ 2 is considered as cut-off for the successive statistical analysis (Dalman et al., 2012; Livak and Schmittgen, 2001).

2.14. Statistics

Student t-test for independent samples was applied to determine the significance of the changes detected between ELF-MF exposed and unexposed groups. The results are reported as mean \pm SD. Values were expressed in % versus CTRL when they are relative to fluorescence or optical density. Statistical analyses were performed using SPSS 19.0 (SPSS Inc., Chicago, IL, USA). P-values < 0.05 were considered significant.

3. Results

3.1. Effects of ELF-MF exposure on breast cancer cell viability and morphology

Following ELF-MF treatment, the number of live cells was significantly reduced in exposed cells compared with unexposed MCF-10A breast cells (respectively 3.2×10^5 live/ 0.3×10^5 dead cells and 2.4×10^5 live/ 0.4×10^5 dead cells) (Fig. 1A). Conversely, exposed MDA-MB-231 breast cancer cells showed a significant increase in live cells but no significant change in the number of dead cells compared with control samples (9.7×10^5 live/ 1.3×10^5 dead cells and 13.1×10^5 live/ 1.6×10^5 dead cells, respectively) (Fig. 1A).

There was not statistically any difference in cell viability between exposed and control MCF-10A cells (101% and 100%, respectively) (Fig. 1B), whereas exposed MDA-MB-231 cells exhibited a significant increase in viable cells compared with their unexposed counterparts (137% and 100%, respectively) (Fig. 1B). The cells density studied at the optical microscope was reduced in exposed MCF-10A compared with unexposed cells (Fig. 1C), as well as the exposed MDA-MB-231 breast cancer cells were denser compared with their control group (Fig. 1C).

Actin microfilament distribution or morphology were studied using Phalloidin staining. In MCF-10A exposed cells there were no substantial differences versus unexposed ones, whereas MDA-MB-231 exposed cells showed increased F-actin organization, F-actin marginalization from the center toward the plasma membrane, and a greater number of pseudopodia compared with controls (Fig. 1D). Filopodia length and density were significantly increased in ELF-MF-exposed MDA-MB-231 breast cancer cells. ELF-MF did not have an effect on the filopodia length and density in MCF-10A breast cells (Fig. 1E).

3.2. ELF-MF exposure induced necrosis in normal breast cells but not in breast cancer cells

Flow cytometry analysis revealed that ELF-MF was able to induce necrosis in MCF-10A breast cells, without any alteration in the early or

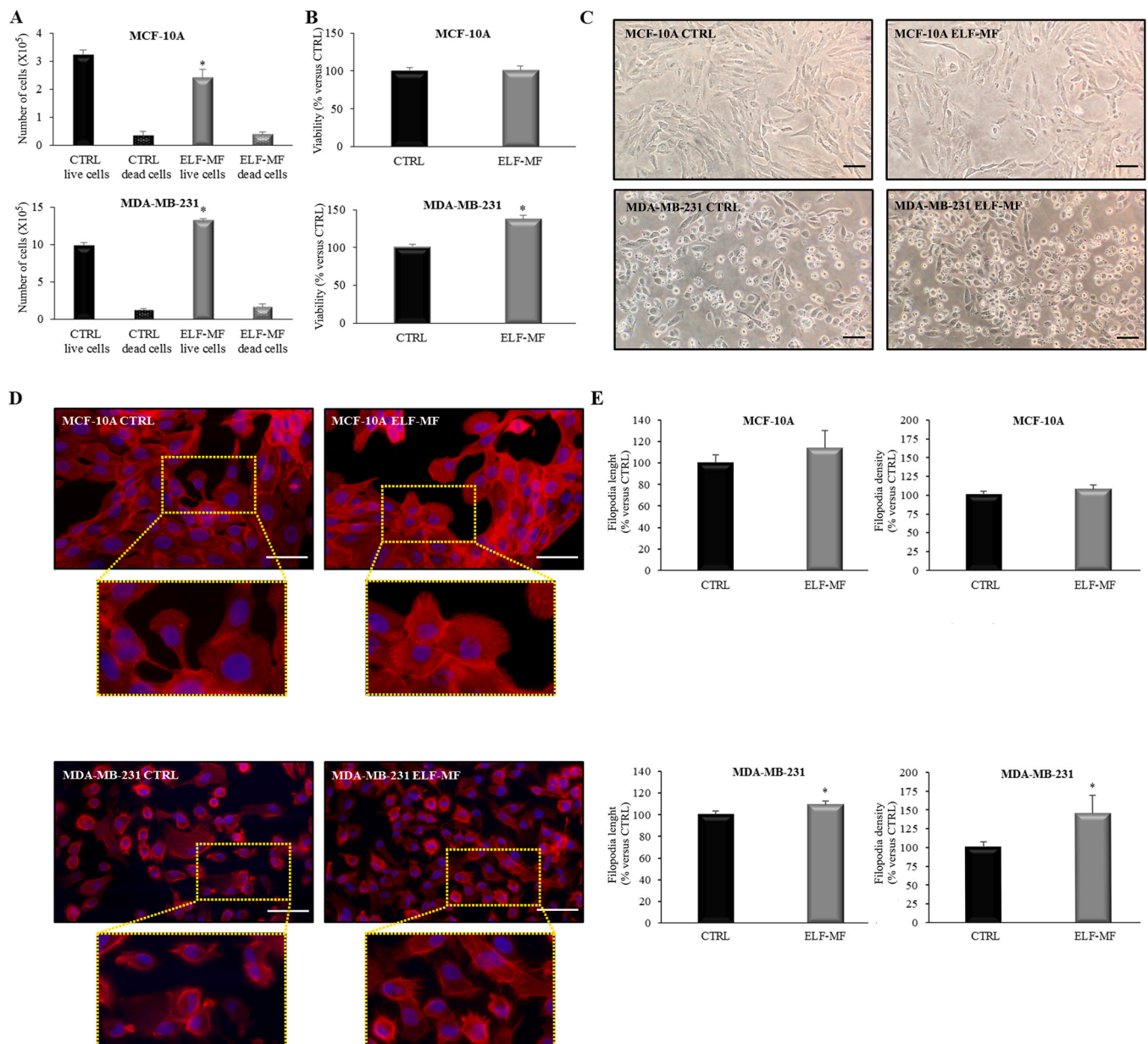


Fig. 1. Changes in live MCF-10A and MDA-MB-231 cell number, viability, and morphology after ELF-MF exposure. All the experiments were independently repeated three times. **A**, Number of live/dead cells in unexposed (CTRL) and ELF-MF-exposed MCF-10A (top, * $P = 0.018$) and MDA-MB-231 (bottom, * $P = 0.001$) cells as determined by the trypan blue assay. Data are mean \pm SD. **B**, Viability of ELF-MF-exposed MCF-10A and MDA-MB-231 (* $P = 0.002$) cells, calculated as a proportion of unexposed cells. Data are mean \pm SD. **C**, Representative images obtained with an inverted microscope showing cell density in unexposed and ELF-MF-exposed MCF-10A cells and unexposed and ELF-MF-exposed MDA-MB-231 cells (scale bar 50 μ m). **D**, Representative images of morphological changes in unexposed and ELF-MF-exposed MCF-10A and unexposed and ELF-MF-exposed MDA-MB-231 cells using TRITC-labeled phalloidin immunostaining (scale bar 50 μ m). **E**, Filopodia length and density in unexposed and ELF-MF-exposed MCF-10A and MDA-MB-231 cells (bottom left, * $P = 0.041$; bottom right, * $P = 0.043$). Data are mean \pm SD and were reported as % versus control (CTRL, 100%).

late apoptosis rate (Figs. 2A and 2C). In contrast, ELF-MF exposure does not induce necrosis and/or apoptosis in MDA-MB-231 cells (Figs. 2B and 2D).

3.3. Mitochondrial morphology and mitochondrial ROS production alteration in normal breast cells and cancer breast cells after ELF-MF exposure

Analysis of cell ultrastructure using transmission electron microscopy revealed a prominent effect of ELF-MF in mitochondria morphology (Figs. 3A and 3B). In both cell lines the alteration in mitochondria was very similar. Mitochondria of ELF-MF treated cells

were consistently larger than controls, the cristae appear to be sparser and the matrix less electron dense compared to the untreated cells. Frequently the mitochondria of ELF-MF treated cells show dilation and loss of matrix. Mitochondrial dysfunctions were often associated with an increased level of mitochondrial ROS, thus we measured mitochondrial reactive oxygen species using MitoSOX fluorescent dye. The results showed that ELF-MF significantly increase the mitochondrial reactive oxygen species production in both MCF-10A and MDA-MB-231 cells, compared to the unexposed cells (Fig. 3C).

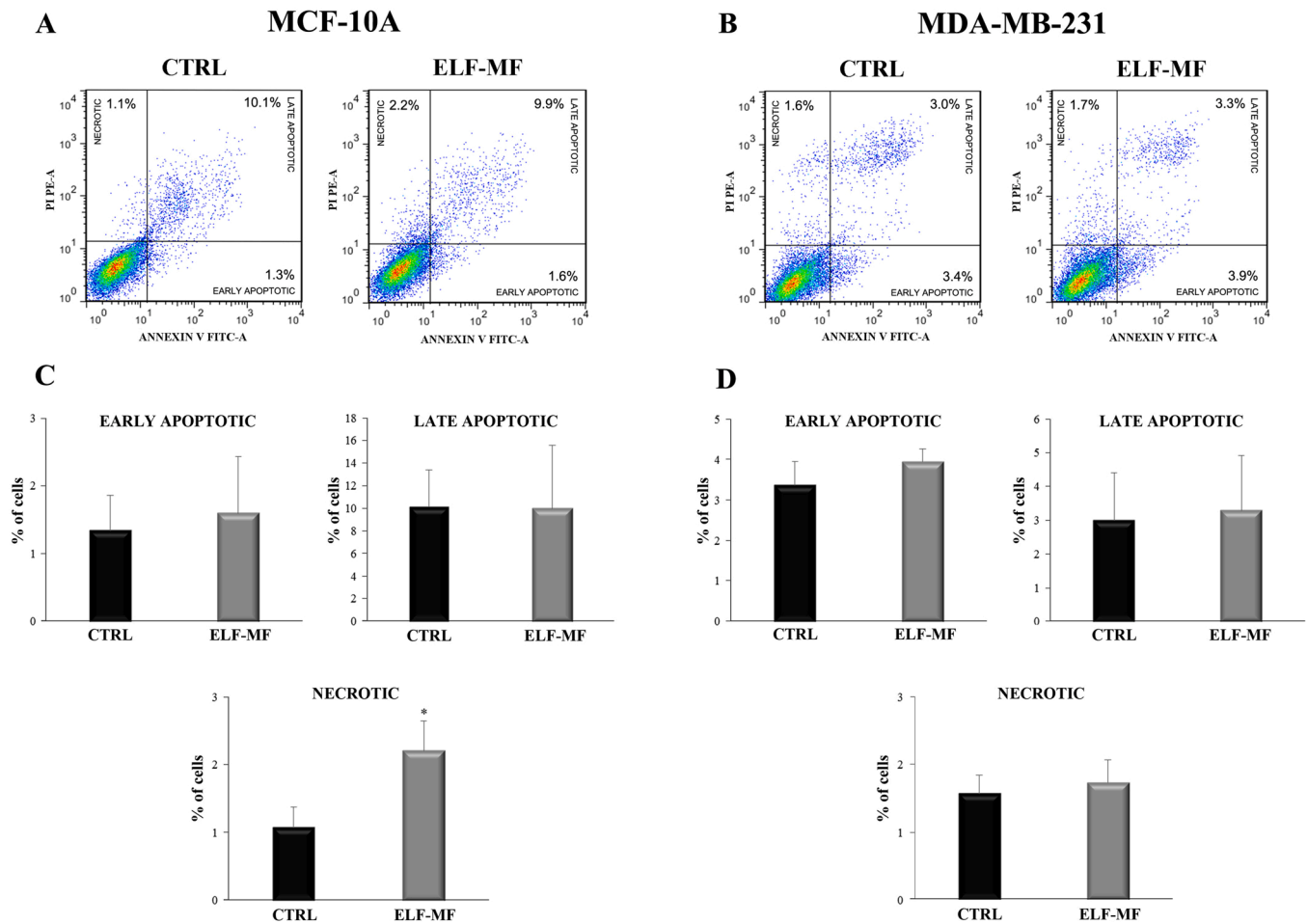


Fig. 2. Mechanism of cell death induced by ELF-MF in MCF-10A and MDA-MB-231 breast cells. MCF-10A **A**, and MDA-MB-231 **B**, cells exposed to ELF-MF were analyzed by flow cytometry using Annexin V and propidium iodide (PI). Representative histograms derived from flow cytometry analysis reported the % of early and late apoptosis and necrosis induced by ELF-MF in MCF10-A **C**, and MDA-MB-231 **D**, cells. Unexposed cells were used as a control (CTRL). Data were expressed as a mean \pm SD from three independent experiments. *P = 0.022 versus control.

3.4. Identification of differentially expressed proteins in ELF-MF treated breast cell lines

Proteome profiling enabled more than 2600 proteins in each cell line to be identified. Shared proteins were 58% (1553/2687) in control and ELF-MF-exposed MCF-10A cells and 53% (1392/2607) in control and ELF-MF-exposed MDA-MB-231 breast cancer cells. The Venn diagram in Fig. 4A shows the intersection of the proteins identified in each group. Hierarchical cluster analysis of protein expression demonstrated a clear separation between exposed and control samples in both cell lines (Fig. 4B). Comparison of control and exposed MCF-10A cells highlighted 242 differentially expressed proteins (FDR $p < 0.05$), whereas comparison of control and exposed MDA-MB-231 cells found 328 differentially expressed proteins (FoldChange ≥ 2 , FDR $p < 0.05$). In exposed MCF-10A cells, 53 of the proteins showing differential expression were upregulated whereas 189 were downregulated. In exposed MDA-MB-231 cells, 242 proteins showing differential expression were upregulated and 86 were downregulated (Fig. 4B). The upregulated and downregulated proteins in MCF-10A and MDA-MB-231 cells were listed in Table S1 (MCF-10A) and Table S2 (MDA-MB-231) of Supplementary material.

GO term enrichment analysis using WebGestalt disclosed that in exposed MCF-10A cells the upregulated genes were significantly enriched in “splicing”, “intracellular protein transport” and “ribonucleoprotein complex”, whereas the downregulated genes were mainly enriched in “focal adhesion”, “mitochondrion”, “ribosome”,

“ribonucleoprotein complex”, and “intracellular transport” (Fig. 4C). In MDA-MB-231 breast cancer cells, ELF-MF exposure resulted in upregulation of genes significantly (adjusted $p < 0.05$) enriched in “focal adhesion”, “mitochondrion”, “ribosome”, “ribonucleoprotein complex” and “intracellular transport”, whereas the downregulated genes were involved in “ribonucleoprotein complex”, “splicing” and “ribosome” (Fig. 4C).

Notably, the GO term “focal adhesion” was consistently upregulated in ELF-MF-exposed MDA-MB-231 breast cancer cells and downregulated in ELF-MF-exposed MCF-10A cells (Fig. 4C). Moreover, results containing the term “splicing” were found in downregulated genes in MDA-MB-231 breast cancer cells and in upregulated genes in MCF-10A cells (Fig. 4C). ITGA6 (Integrin α -6), GNB2 (guanine nucleotide-binding protein G(I)/G(S)/G(T) subunit beta-2) and RPS14 (ribosomal protein S14), belonging to the “focal adhesion” cellular component, were upregulated in exposed MDA-MB-231 breast cancer cells, and downregulated in exposed MCF-10A cells. As regards “mitochondrion”, ECHS1 (Enoyl-CoA hydratase), MAVS (mitochondrial anti-viral signaling protein), OGDH (2-oxoglutarate dehydrogenase), PCK2 (phosphoenolpyruvate carboxykinase [GTP]), PPA2 (inorganic pyrophosphatase 2), SFXN1 (sideroflexin-1), TIMM8A (mitochondrial import inner membrane translocase subunit Tim8 A), TOMM22 (mitochondrial import receptor subunit TOMM22 homolog), and TUFM (elongation factor Tu) were upregulated in exposed MDA-MB-231 cells and downregulated in exposed MCF10-A cells. Significantly differentially expressed proteins were also identified by Linear discriminant analysis

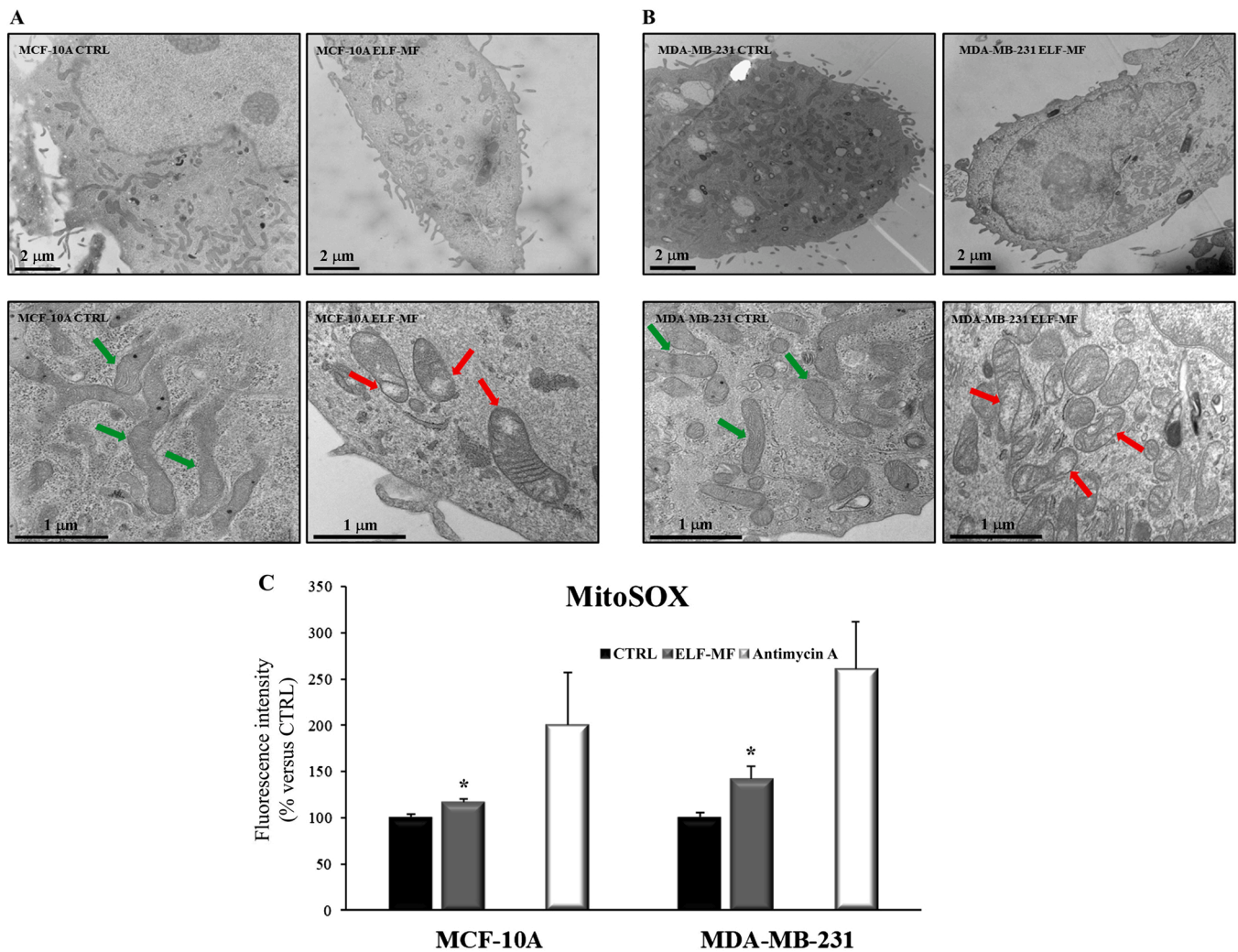


Fig. 3. Ultrastructure of cells exposed to ELF-MF and mitochondrial superoxide production using MitoSOX RED fluorescent dye. **A**, MCF-10A and **B**, MDA-MB-231 cell monolayers imaged at the transmission electron microscope. Overall cell shape and size are not apparently altered by the treatment as shown in the upper panel at low magnification. At higher magnification (lower panels) both cell lines show an enlargement of mitochondria (green arrows) upon ELF-MF treatment (red arrows). Treated cells mitochondria also show vacuoles denoting abnormal function. **C**, Levels of mitochondrial superoxide were quantified by a plate reader, and normalized for number of cells, quantified using Hoechst 33342 DNA-binding dye. MCF-10A and MDA-MB-231 cells treated with Antimycin A were used as a positive control. Results were expressed in % versus the unexposed cells (CTRL), the data are reported as a mean \pm SD and derived from three independent experiments. MCF-10A, * $P = 0.007$; MDA-MB-231, * $P = 0.009$.

(LDA) effect size (LefSe) analysis. This analysis was more stringent than that performed by Perseus, in fact fewer genes were highlighted (Supplementary material, Fig. S1). In particular, the new analysis on MCF-10A cells highlighted 50 down-regulated proteins instead of 189 in the previous analysis, and 97 up-regulated proteins instead of 242 in MDA-MB-231 cells. On the contrary, the number of proteins up-regulated in MCF-10A cells and those down-regulated in MDA-MB-231 cells remained unchanged. By performing the enrichment analysis on these LefSe-derived lists we obtained the same pathways already shown in Fig. 4C.

3.5. Adhesion, migration and invasion abilities of normal breast cells and breast cancer cells altered by ELF-MF exposure

After exposure to ELF-MF, MDA-MB-231 breast cancer cells showed a significantly lower attachment tendency to the 96 well plate surface, compared with the unexposed MDA-MB-231 cells (CTRL) (Fig. 5A). MCF-10A human breast epithelial cells, which are adhesion dependent for their survival, showed no changes in adhesion after ELF-MF exposure (Fig. 5A). The ability of cell-matrix migration and invasion was detected

using transwell assay without and with GelTrex coated insert, respectively. MCF-10A cells showed a significant reduction in their migration ability after ELF-MF exposure compared with control cells (Figs. 5B and 5C). After exposure to ELF-MF, MDA-MB-231 cells showed a significant increase in cell invasion compared with unexposed cells (Figs. 5D and 5E).

3.6. Analysis of regulatory factors and pluripotency factor genes in ELF-MF-exposed MDA-MB-231 breast cancer cells

To further elucidate the molecular mechanisms that could be affected by ELF-MF exposure and explain the altered expression of the proteins identified, we investigated the most significantly enriched transcription factors (TFs). Use of the Enrichr webtool on differentially expressed protein list obtained by analysis with Perseus software allowed the identification of several significantly enriched TFs. Four of these TFs, belonging to the pluripotency transcription factors KLF4 (Krueppel-like factor 4), STAT3 (Signal Transducer and activator of transcription 3), BCLAF1 (Bcl2-associated transcription factor 1), and NR2C2 (Nuclear receptor subfamily 2 group C member 2), and, were

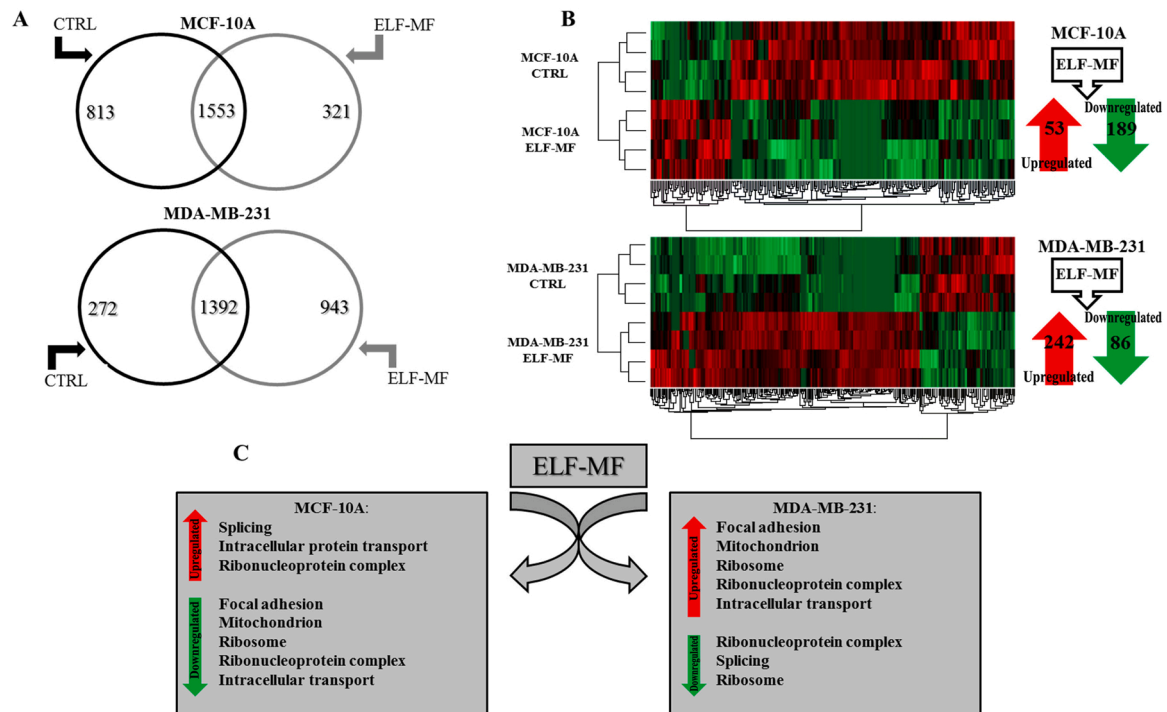


Fig. 4. Proteomic characterization of MCF-10A and MDA-231 cells not exposed and exposed to ELF-MF. **A**, The Venn diagram shows the intersection of the proteins identified in unexposed and ELF-MF-exposed MCF-10A cells (MCF-10A CTRL and MCF-10A ELF-MF) and in unexposed and ELF-MF-exposed MDA-MB-231 cells (MDA-MB-231 CTRL and MDA-MB-231 ELF-MF). **B**, Hierarchical clustering of proteins with differential expression between ELF-MF exposed and control (CTRL) MCF-10A and MDA-MB-231 breast cells. The intensity of color represents the value of upregulation (red) or downregulation (green). ELF-MF exposed MCF-10A cells exhibited 53 upregulated and 189 downregulated proteins compared with control cells while exposed MDA-MB-231 cells showed 242 upregulated and 86 downregulated proteins compared with the control cells. **C**, Gene Ontology term enrichment analysis using the WebGestalt tool disclosed that the genes up- and downregulated in each exposed cell sample compared with the control cells belonged to specific GO terms. Red and green arrows indicate Gene Ontology terms enriched in upregulated and downregulated genes.

found exclusively in the TFs lists of genes downregulated in MCF-10A cells and upregulated in MDA-MB-231 cells. ELF-MF exposure induced significant down-regulation of *STAT3*, *BCLAF1*, and *NR2C2* mRNA in exposed MCF-10A cells compared to control cells, without alteration in the *KLF4* gene expression (Fig. 6A). On the contrary, in MDA-MB-231 breast cancer cells, ELF-MF exposure induced up-regulation of pluripotency factors *KLF4*, *STAT3*, *BCLAF1* and *NR2C2* genes, compared to control cells (Fig. 6A).

Five TFs, UBTF (Nucleolar transcription factor 1), USF1 (Upstream stimulatory factor 1), CEBPD (CCAAT/enhancer-binding protein delta), ZMIZ1 (Zinc finger domain-containing protein 1), and CHD1 (Chromodomain-helicase-DNA-binding protein 1), were found in the TF lists of genes upregulated in MCF-10A cells and downregulated in MDA-MB-231 cells. The mRNA expression levels of *UBTF*, *USF1*, *CEBPD*, *ZMIM1* and *CHD1* transcription factors, do not change between MCF-10A and MDA-MB-231 ELF-MF exposed and unexposed cells (Fig. 6B).

The Enrichr's predictions on the protein lists obtained from the LEfSe confirmed NR2C2, STAT3 and USF1 as significantly enriched TFs.

4. Discussion

ELF-MF have been demonstrated to act as stressors of cellular physiology (Bernard et al., 2008; Koeman et al., 2013; Koziorowska et al., 2017). They can modify cell morphology and affect intracellular mechanisms while inducing different responses in relation to cell type (Giorgi and Del Re, 2021; Mattsson and Simkó, 2014). Although it appears that ELF-MF are unable to induce DNA damage directly (Valberg et al., 1997; Wang et al., 2019), the molecular mechanisms activated by this exogenous stressor are still to be elucidated.

Exposure to 1 mT 50 Hz ELF-MF for 4 h reduced the proliferation rate of MCF-10A normal human mammary epithelial cells but did not

affect the number of dead cells or cell viability compared to control cultures. Conversely, ELF-MF exposure increased the number of proliferating cells and cell viability in MDA-MB-231 breast cancer cells. Lee et al. reported a similar effect on MCF-10A cell proliferation (Lee et al., 2015), while Hong et al. found no differences (Hong et al., 2012). Regarding MDA-MB-231 breast cancer cells, Masoudi-Khoram & Abdolmaleki found a reduced cell viability and an increased apoptotic rate of cells exposed to 50 Hz EMF at 20 mT for 3 h/day for up to four days (Masoudi-Khoram and Abdolmaleki, 2022). Wang and al. found a strong inhibition of MDA-MB-231 cell proliferation after a 6 h switching, 7.83 ± 0.3 Hz, 1 mT ELF-MF exposure for two consecutive days, while viability increased with increases in the applied frequency (Wang et al., 2021). A significant increase in apoptosis and reduction of proliferation was seen in MDA-MB-231 cells exposed to 1 Hz, 100 mT ELF-MF by Nezamtaheri and al. (Nezamtaheri et al., 2022). The increase in MDA-MB-231 cell viability obtained with our ELF-MF exposure is not in contrast with data from other studies. Indeed, an inhibitory effect on MDA-MB-231 cell growth was observed after ELF-MF exposures with higher magnetic flux density and/or lower frequency than those used in our study. It is in line with the increasing evidences that cellular growth response is closely related to ELF-MF exposure characteristics (i.e. frequency, intensity, duration, continuous or switching) (Focke et al., 2010; Makinistian et al., 2019; Martínez et al., 2012, 2016; Nezamtaheri et al., 2022; Wang et al., 2021).

The phalloidin staining revealed an increased organization of F-actin only in MDA-MB-231 breast cancer cells exposed to ELF-MF. The actin filaments are associated with cell proliferation (Tavares et al., 2017), cellular adhesion (Dugina et al., 2019), and cell reprogramming (Guo et al., 2014). This phenomena is in-line to similar results obtained in other types of cells exposed to ELF-MF (Santoro et al., 1997; Shen et al., 2016; Zhang et al., 2018). The increased filopodia length and density in

ADHESION

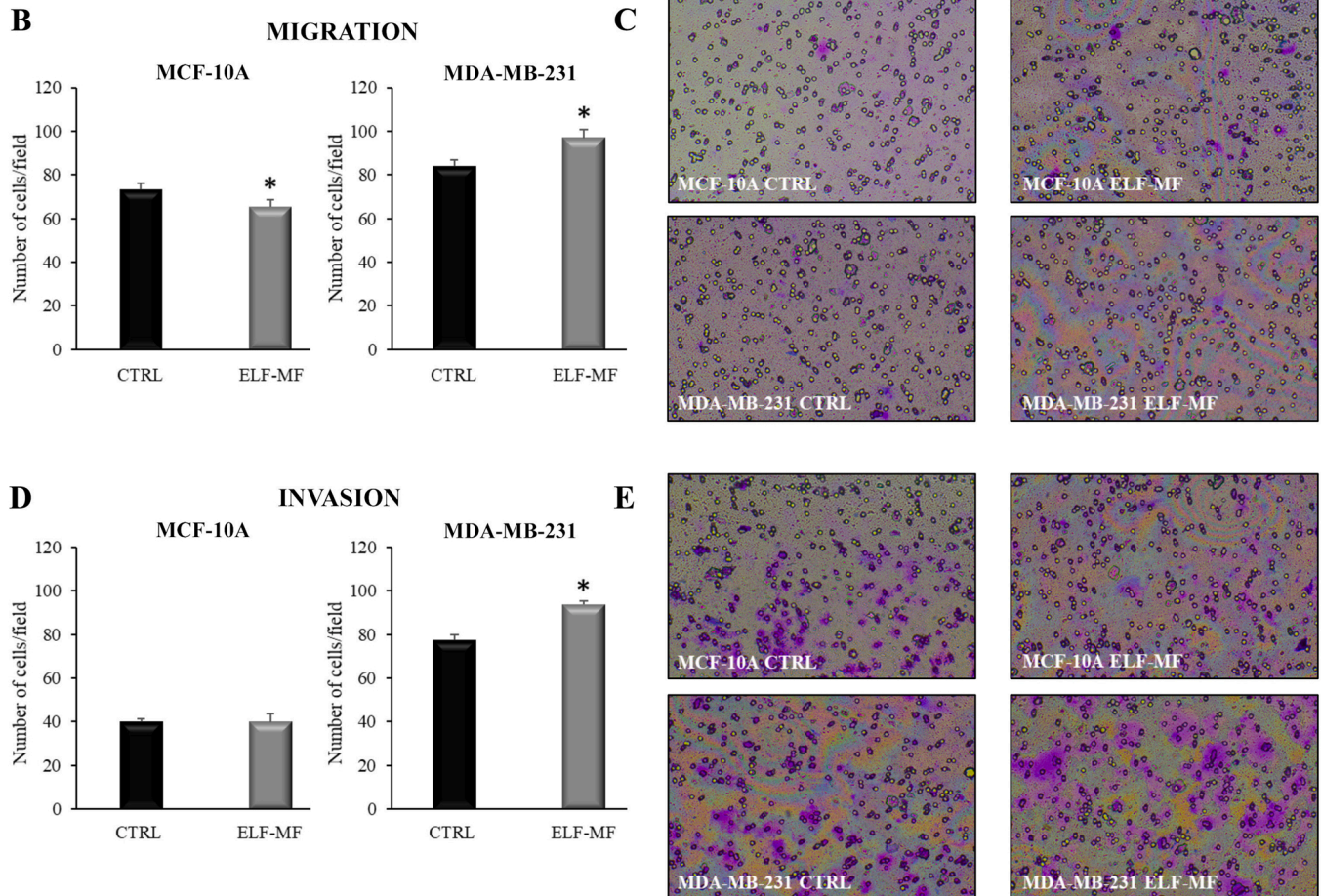
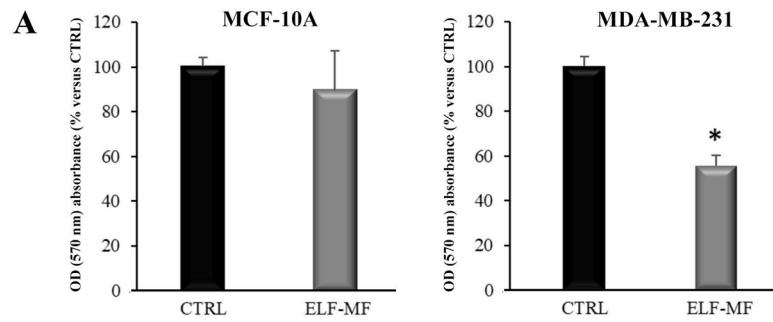


Fig. 5. Cell adhesion, migration, and invasion of MCF-10A and MDA-MB-231 cell lines exposed to ELF-MF. **A**, Adhesion assay: MCF-10A and MDA-MB-231 cells were exposed to ELF-MF for 4 h and after 96 h were seeded into 96 wells for 1 h. Crystal violet was used to stain attached cells that were subsequently analyzed by a plate reader. Results are reported as % of optical absorbance of adherent cells compared with ELF-MF unexposed cells (CTRL). * $P = 0.001$. **B** and **C**, Transwell migration assay: migrating cells were fixed and stained with crystal violet and the number of migrating cells was analyzed in five different fields. MCF-10A, * $P = 0.045$; MDA-MB-231, * $P = 0.012$. **D** and **E**, Transwell invasion assay: MCF-10A and MDA-MB-231 cells after exposure to ELF-MF were seeded on Transwell inserts coated with GelTrex. Cells were fixed, stained, and counted as described above. * $P = 0.001$. Data and images are relative of three independent experiments. Data are reported as a mean \pm SD.

MDA-MB-231 breast cancer cells exposed to ELF-MF suggests features of migrating/invading cancer cells (Jacquemet et al., 2017).

The analysis of cell ultrastructure using transmission electron microscopy revealed an effect of EMF-MF in mitochondria morphology on both breast cell lines analyzed. Mitochondria are cellular components that respond sooner to cellular stimuli showing ultrastructural alterations. Swelling of mitochondria with a dilatation of the intercris- tae space is induced by hypoxia or hyposmosis (Arismendi-Morillo, 2009) and enlarged mitochondria has been associated with aging or oxidative

stress (Duranova et al., 2020). Increased mitochondrial activity and oxidative stress were associated to ELF-MF exposure (Luukkonen et al., 2014; Santini et al., 2018; Zhang et al., 2017). This evidence is supported by our data, ELF-MF promoted an increase of mitochondrial reactive oxygen species (ROS) production in both MCF-10A breast cells and MDA-MB-231 breast cancer cells. In cancer cells, ELF-MF may induce redox-responsive pathways, associated to proliferative or survival advantage (Falone et al., 2017).

Some studies of various cell types have found that ELF-MF can

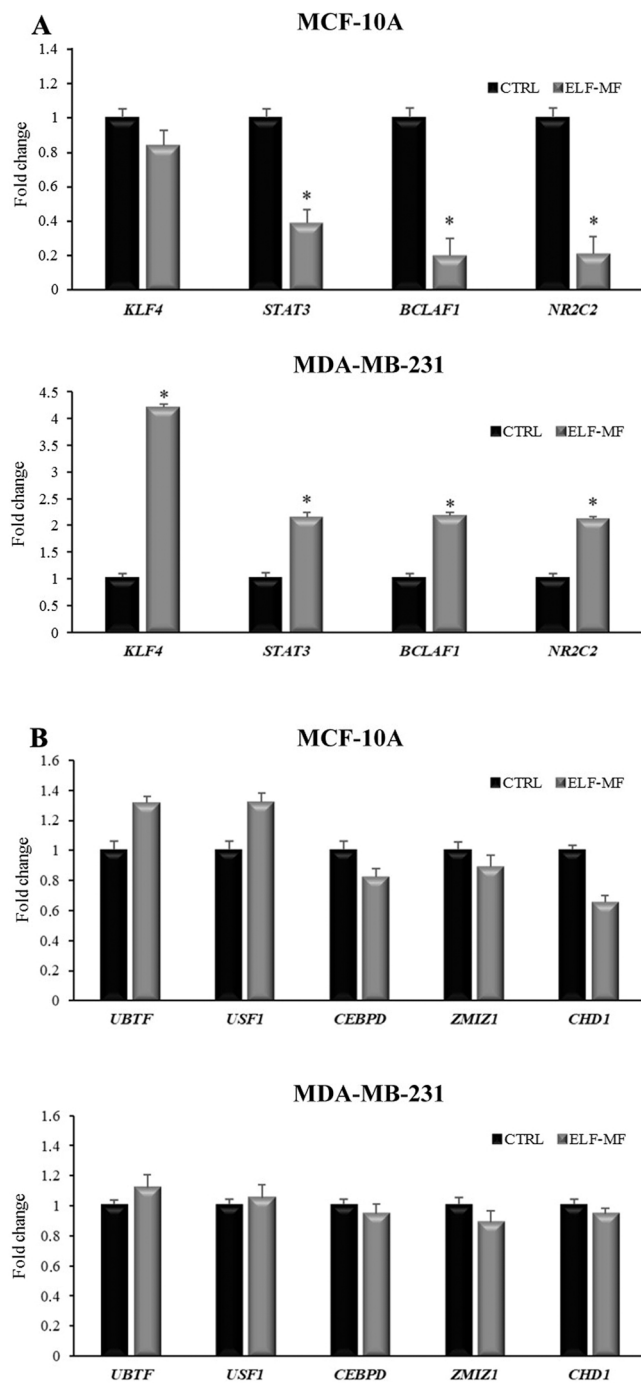


Fig. 6. Transcription Factors (TFs) involved in the ELF-MF response in MCF-10A and MDA-MB-231 cells. **A**, mRNA differential expression of *KLF4*, *STAT3*, *BCLAF1* and *NR2C2* pluripotency TFs in ELF-MF-exposed MCF-10A cells (MCF-10A ELF-MF, *STAT3* **P* = 0.001, *BCLAF1* and *NR2C2* **P* < 0.001) compared to their controls (MCF-10A CTRL) and in ELF-MF-exposed MDA-MB-231 cells (MDA-MB-231 ELF-MF, **P* < 0.001), compared with their controls (MDA-MB-231 CTRL). **B**, mRNA expression levels of *UBTF*, *USF1*, *CEBPD*, *ZMIZ1* and *CHD1* TFs, genes expression analysis. Data are expressed as fold change ($2^{-\Delta\Delta Ct}$) relative to unexposed cells. Data are mean \pm SD and are from three independent experiments.

modify membrane protein distribution and phosphorylation by altering intracellular signaling pathways (Hu et al., 2001; Kapri-Pardes et al., 2017; Park et al., 2013). These phenomena induce activation of an altered transcription/translation of the genes that in live cells regulate a variety of effects such as proliferation, migration, redox-responsive

intracellular signaling, and differentiation potential (Falone et al., 2018; Giorgi and Del Re, 2021; Guerriero and Ricevuti, 2016; Manzella et al., 2015; Xu et al., 2020). Dysregulation of these cell properties is known to promote carcinogenesis and cancer progression. Our study shows that ELF-MF alter the expression of some key proteins in both MCF-10A cells and MDA-MB-231 cancer cells. GO term enrichment analysis showed that the molecular mechanisms implicated in the response to ELF-MF are similar but opposite in the two cell lines. ELF-MF downregulated “focal adhesion” and “mitochondrion” in MCF-10A cells and upregulated them in MDA-MB-231 cancer cells.

As regards “focal adhesion”, ITGA6, GNB2 and RPS14 were down-regulated in MCF-10A cells and upregulated in MDA-MB-231 breast cancer cells exposed to ELF-MF. ITGA6 has been reported to play a pivotal role in breast cancer invasion and metastasis (Brooks et al., 2016) and to be an independent prognostic factor in estrogen receptor-negative disease (Ali et al., 2011). The G family protein GNB2 has been implicated in the proliferation, metastasis, and response to treatment of cutaneous melanoma (Chen et al., 2020), prostate cancer (Zhang et al., 2019), and breast cancer (Mittal et al., 2020).

After ELF-MF exposure, ECHS, MAVS, OGDH, PCK2, PPA2, SFXN1, TIMM8A, TOMM22 and TUFM proteins, related to “mitochondrion” in GO term enrichment analysis, were downregulated in MCF-10A cells and upregulated in MDA-MB-231 breast cancer cells., which has been implicated in the ability of metastatic breast cells to alter their metabolism in response to environmental stress and to induce epithelial to mesenchymal transition and metastasis (Simões et al., 2015).

Transcription factors have a key role in the regulation of the physiological and pathological molecular mechanisms of breast cells. In our study, exposure to ELF-MF induced respectively up-regulation and down-regulation of 5 TFs (*UBTF*, *USF1*, *CEBPD*, *ZMIZ1* and *CHD1*) in MCF-10A and MDA-MB-231 cells. *CEBPD* is involved in the inflammatory response and has been reported to enhance *IL6* gene transcription (Balamurugan et al., 2019), whereas *ZMIZ1* acts as a transcriptional coactivator and has been reported to activate *NOTCH1* target genes, including *C-MYC* (Rakowski et al., 2013). In contrast, the expression levels of *KLF4*, *STAT3*, *BCLAF1*, and *NR2C2* were significantly reduced in exposed MCF-10A cells and significantly increased in exposed MDA-MB-231 breast cancer cells. Notably, *KLF4* is a key regulator of cell proliferation, differentiation, and transformation and takes part in oncogenesis and breast cancer development through a complex and not completely elucidated mechanism (Taracha-Wisniewska et al., 2020). *STAT3* has a key role in triple-negative breast cancer pathogenesis, progression and metastasis as a signal transducer and transcription activator capable of inducing cell survival, proliferation, and migration (Qin et al., 2019). In this scenario, we tested the mRNA expression levels of genes associated with pluripotency, like *KLF4*, *STAT3*, *BCLAF1* and *NR2C2*. Interestingly, in MDA-MB-231 cells ELF-MF exposure induced significant up-regulation of all these genes associated with the pluripotency and proliferative potential. In contrast, in MCF-10A breast cells the expression levels of *STAT3*, *BCLAF1* and *NR2C2* were significantly decreased.

5. Conclusions

Our findings showed several proteins and cellular targets through which an exposure to 1 mT 50 Hz ELF-MF elicited changes in cell biology and behavior of MDA-MB-231 breast cancer cells. The main pathways involved were relative to focal adhesion, mitochondrion and cellular reprogramming. Exposed MDA-MB-231 breast cancer cells showed modifications in proteomic profile together with changes in cell viability, cellular morphology, oxidative stress response, adhesion, migration and invasion cell abilities. Further studies investigating in vivo effects of 1 mT 50 Hz ELF-MF exposure on breast cells are needed.

Funding

This research was supported by the Polytechnic University of Marche, Ancona, Italy.

CRedit authorship contribution statement

Raffaella Lazzarini: Conceptualization, Investigation, Data curation, Formal analysis, Writing – original draft. **Maria Eléxpuru Zabaleta:** Investigation, Formal analysis. **Francesco Piva:** Conceptualization, Resources. **Matteo Giulietti:** Methodology, Data curation, Formal analysis. **Gianluca Fulgenzi:** Methodology, Investigation. **Maria Fiorella Tartaglione:** Investigation. **Laura Zingaretti:** Data curation, Formal analysis. **Adriano Tagliabracchi:** Methodology; **Matteo Valentino:** Data curation, Formal analysis; **Lory Santarelli:** Supervision, Writing – review & editing. **Massimo Bracci:** Conceptualization, Methodology, Writing – original draft, Supervision, Project administration.

Declaration of Competing Interest

The authors declare that they have no known competing financial interests or personal relationships that could have appeared to influence the work reported in this paper.

Data Availability

The raw proteomic data have been uploaded to the jPOST repository with the identifiers JPST002039 (jPOST) and PXD040120 (ProteomeXchange).

Acknowledgments

We thank Dr. Veronica Ciarapica for her precious aid in the pilot experiments, Dr. Alice Marzetti and Dr. Martina Chierchiè for their kind support in the laboratory, and Dr. Paolo Soffientini (Cogentech Srl, Italy) for the technical support.

Appendix A. Supporting information

Supplementary data associated with this article can be found in the online version at [doi:10.1016/j.ecoenv.2023.114650](https://doi.org/10.1016/j.ecoenv.2023.114650).

References

- Abbott, J.J., 2015. Parametric design of tri-axial nested Helmholtz coils. *Rev. Sci. Instrum.* 86, 054701.
- Ali, H.R., et al., 2011. Cancer stem cell markers in breast cancer: pathological, clinical and prognostic significance. *Breast Cancer Res* 13, R118.
- Arismendi-Morillo, G., 2009. Electron microscopy morphology of the mitochondrial network in human cancer. *Int J. Biochem Cell Biol.* 41, 2062–2068.
- Baek, S., et al., 2014. Electromagnetic fields mediate efficient cell reprogramming into a pluripotent state. *ACS Nano* 8, 10125–10138.
- Balamurugan, K., et al., 2019. C/EBP δ links IL-6 and HIF-1 signaling to promote breast cancer stem cell-associated phenotypes. *Oncogene* 38, 3765–3780.
- Bernard, N., et al., 2008. Assessing the potential leukemogenic effects of 50 Hz magnetic fields and their harmonics using an animal leukemia model. *J. Radiat. Res* 49, 565–577.
- Brooks, D.L., et al., 2016. ITGA6 is directly regulated by hypoxia-inducible factors and enriches for cancer stem cell activity and invasion in metastatic breast cancer models. *Mol. Cancer* 15, 26.
- Carpenter, D.O., 2019. Extremely low frequency electromagnetic fields and cancer: How source of funding affects results. *Environ. Res* 178, 108688.
- Chan, K.T., et al., 2009. FAK alters invadopodia and focal adhesion composition and dynamics to regulate breast cancer invasion. *J. Cell Biol.* 185, 357–370.
- Chen, J., et al., 2020. Identification of key genes involved in the pathogenesis of cutaneous melanoma using bioinformatics analysis. *J. Int Med Res* 48, 300060519895867.
- Corominas-Faja, B., et al., 2013. Nuclear reprogramming of luminal-like breast cancer cells generates Sox2-overexpressing cancer stem-like cellular states harboring transcriptional activation of the mTOR pathway. *Cell Cycle* 12, 3109–3124.
- Cox, J., et al., 2011. Andromeda: a peptide search engine integrated into the MaxQuant environment. *J. Proteome Res* 10, 1794–1805.
- Cox, J., Mann, M., 2008. MaxQuant enables high peptide identification rates, individualized p.p.b.-range mass accuracies and proteome-wide protein quantification. *Nat. Biotechnol.* 26, 1367–1372.
- Dalman, M.R., et al., 2012. Fold change and p-value cutoffs significantly alter microarray interpretations. *BMC Bioinforma.* 13 (Suppl 2), S11.
- Du, L., et al., 2014. Extremely low frequency magnetic fields inhibit adipogenesis of human mesenchymal stem cells. *Bioelectromagnetics* 35, 519–530.
- Dugina, V.B., et al., 2019. Biological role of actin isoforms in mammalian cells. *Biochem. (Mosc.)* 84, 583–592.
- Duranova, H., et al., 2020. Mitochondria: a worthwhile object for ultrastructural qualitative characterization and quantification of cells at physiological and pathophysiological states using conventional transmission electron microscopy. *Acta Histochem* 122, 151646.
- Falone, S., et al., 2017. Power frequency magnetic field promotes a more malignant phenotype in neuroblastoma cells via redox-related mechanisms. *Sci. Rep.* 7, 11470.
- Falone, S., et al., 2018. Extremely low-frequency magnetic fields and redox-responsive pathways linked to cancer drug resistance: insights from co-exposure-based in vitro studies. *Front Public Health* 6, 33.
- Feng, Y., et al., 2018. Breast cancer development and progression: risk factors, cancer stem cells, signaling pathways, genomics, and molecular pathogenesis. *Genes Dis.* 5, 77–106.
- Focke, F., et al., 2010. DNA fragmentation in human fibroblasts under extremely low frequency electromagnetic field exposure. *Mutat. Res* 683, 74–83.
- Giorgi, G., Del Re, B., 2021. Epigenetic dysregulation in various types of cells exposed to extremely low-frequency magnetic fields. *Cell Tissue Res* 386, 1–15.
- Guerrero, F., Ricevuti, G., 2016. Extremely low frequency electromagnetic fields stimulation modulates autoimmunity and immune responses: a possible immunomodulatory therapeutic effect in neurodegenerative diseases. *Neural Regen. Res* 11, 1888–1895.
- Guo, J., et al., 2014. Actin stress in cell reprogramming. *Proc. Natl. Acad. Sci. USA* 111, E5252–E5261.
- Hong, G., et al., 2014. Separate enrichment analysis of pathways for up- and downregulated genes. *J. R. Soc. Interface* 11, 20130950.
- Hong, M.N., et al., 2012. Extremely low frequency magnetic fields do not elicit oxidative stress in MCF10A cells. *J. Radiat. Res* 53, 79–86.
- Hu, G.L., et al., 2001. ELF magnetic field inhibits gap junctional intercellular communication and induces hyperphosphorylation of connexin43 in NIH3T3 cells. *Bioelectromagnetics* 22, 568–573.
- Jacquemet, G., et al., 2017. FiloQuant reveals increased filopodia density during breast cancer progression. *J. Cell Biol.* 216, 3387–3403.
- Jacquemet, G., et al., 2019. Filopodia Quantification Using FiloQuant. *Methods Mol. Biol.* 2040, 359–373.
- Kapri-Pardes, E., et al., 2017. Activation of signaling cascades by weak extremely low frequency electromagnetic fields. *Cell Physiol. Biochem* 43, 1533–1546.
- Koeman, T., et al., 2013. Occupational exposure to extremely low-frequency magnetic fields and cardiovascular disease mortality in a prospective cohort study. *Occup. Environ. Med* 70, 402–407.
- Koziorowska, A., et al., 2017. Electromagnetic fields with frequencies of 5, 60 and 120 Hz affect the cell cycle and viability of human fibroblast BJ in vitro. *J. Biol. Regul. Homeost. Agents* 31, 725–730.
- Kulak, N.A., et al., 2014. Minimal, encapsulated proteomic-sample processing applied to copy-number estimation in eukaryotic cells. *Nat. Methods* 11, 319–324.
- Lee, H.C., et al., 2015. Effect of extremely low frequency magnetic fields on cell proliferation and gene expression. *Bioelectromagnetics* 36, 506–516.
- Lee, H.J., et al., 2012. Combined effects of 60 Hz electromagnetic field exposure with various stress factors on cellular transformation in NIH3T3 cells. *Bioelectromagnetics* 33, 207–214.
- Lieblein, J.C., et al., 2008. STAT3 can be activated through paracrine signaling in breast epithelial cells. *BMC Cancer* 8, 302.
- Livak, K.J., Schmittgen, T.D., 2001. Analysis of relative gene expression data using real-time quantitative PCR and the 2(-Delta Delta C(T)) Method. *Methods* 25, 402–408.
- Luo, M., Guan, J.L., 2010. Focal adhesion kinase: a prominent determinant in breast cancer initiation, progression and metastasis. *Cancer Lett.* 289, 127–139.
- Luukkonen, J., et al., 2014. Induction of genomic instability, oxidative processes, and mitochondrial activity by 50Hz magnetic fields in human SH-SY5Y neuroblastoma cells. *Mutat. Res* 760, 33–41.
- Maes, A., Verschaeve, L., 2016. Genetic damage in humans exposed to extremely low-frequency electromagnetic fields. *Arch. Toxicol.* 90, 2337–2348.
- Maffei, M.E., 2022. Magnetic fields and cancer: epidemiology, cellular biology, and therapeutics. *Int J. Mol. Sci.* 23.
- Makinistian, L., et al., 2019. A high throughput screening system of coils for ELF magnetic fields experiments: proof of concept on the proliferation of cancer cell lines. *BMC Cancer* 19, 188.
- Manzella, N., et al., 2015. Circadian gene expression and extremely low-frequency magnetic fields: an in vitro study. *Bioelectromagnetics* 36, 294–301.
- Martínez, M.A., et al., 2012. The proliferative response of NB69 human neuroblastoma cells to a 50 Hz magnetic field is mediated by ERK1/2 signaling. *Cell Physiol. Biochem* 29, 675–686.
- Martínez, M.A., et al., 2016. Power frequency magnetic fields affect the p38 MAPK-mediated regulation of NB69 cell proliferation implication of free radicals. *Int J. Mol. Sci.* 17, 510.
- Masoudi-Khoram, N., Abdolmaleki, P., 2022. Effects of repeated exposure to 50 Hz electromagnetic field on breast cancer cells. *Electro Biol. Med* 41, 44–51.

- Mattsson, M.O., Simkó, M., 2012. Is there a relation between extremely low frequency magnetic field exposure, inflammation and neurodegenerative diseases? A review of in vivo and in vitro experimental evidence. *Toxicology* 301, 1–12.
- Mattsson, M.O., Simkó, M., 2014. Grouping of experimental conditions as an approach to evaluate effects of extremely low-frequency magnetic fields on oxidative response in in vitro studies. *Front Public Health* 2, 132.
- Mittal, L., et al., 2020. High-throughput, label-free quantitative proteomic studies of the anticancer effects of electrical pulses with turmeric silver nanoparticles: an in vitro model study. *Sci. Rep.* 10, 7258.
- Nezamtaheri, M.S., et al., 2022. Differential biological responses of adherent and non-adherent (cancer and non-cancerous) cells to variable extremely low frequency magnetic fields. *Sci. Rep.* 12, 14225.
- Núñez-Enríquez, J.C., et al., 2020. Extremely low-frequency magnetic fields and the risk of childhood B-lineage acute lymphoblastic leukemia in a City with high incidence of leukemia and elevated exposure to ELF magnetic fields. *Bioelectromagnetics* 41, 581–597.
- Park, J.E., et al., 2013. Electromagnetic fields induce neural differentiation of human bone marrow derived mesenchymal stem cells via ROS mediated EGFR activation. *Neurochem Int* 62, 418–424.
- Qin, J.J., et al., 2019. STAT3 as a potential therapeutic target in triple negative breast cancer: a systematic review. *J. Exp. Clin. Cancer Res* 38, 195.
- Rakowski, L.A., et al., 2013. Convergence of the ZMIZ1 and NOTCH1 pathways at C-MYC in acute T lymphoblastic leukemias. *Cancer Res* 73, 930–941.
- 2002 International Agency for Research on Cancer Non-ionizing radiation, part 1: static and extremely low-frequency (ELF) electric and magnetic fields. IARC Monogr. Eval. Carcinog. Risks Hum. 80, 2002, 1–395.
- Rappsilber, J., et al., 2003. Stop and go extraction tips for matrix-assisted laser desorption/ionization, nanoelectrospray, and LC/MS sample pretreatment in proteomics. *Anal. Chem.* 75, 663–670.
- Razavi, S.M., et al., 2017. Comprehensive functional enrichment analysis of male infertility. *Sci. Rep.* 7, 15778.
- Ross, C.L., 2017. The use of electric, magnetic, and electromagnetic field for directed cell migration and adhesion in regenerative medicine. *Biotechnol. Prog.* 33, 5–16.
- Santini, S.J., et al., 2018. Role of mitochondria in the oxidative stress induced by electromagnetic fields: focus on reproductive systems. *Oxid. Med Cell Longev.* 2018, 5076271.
- Santoro, N., et al., 1997. Effect of extremely low frequency (ELF) magnetic field exposure on morphological and biophysical properties of human lymphoid cell line (Raji). *Biochim Biophys. Acta* 1357, 281–290.
- Segata, N., et al., 2011. Metagenomic biomarker discovery and explanation. *Genome Biol.* 12, R60.
- Shen, Y., et al., 2016. Exposure to 50Hz-sinusoidal electromagnetic field induces DNA damage-independent autophagy. *Int J. Biochem Cell Biol.* 77, 72–79.
- Simões, R.V., et al., 2015. Metabolic plasticity of metastatic breast cancer cells: adaptation to changes in the microenvironment. *Neoplasia* 17, 671–684.
- Sulpizio, M., et al., 2011. Molecular basis underlying the biological effects elicited by extremely low-frequency magnetic field (ELF-MF) on neuroblastoma cells. *J. Cell Biochem* 112, 3797–3806.
- Taracha-Wisniewska, A., et al., 2020. Recent discoveries on the involvement of krüppel-like factor 4 in the most common cancer types. *Int J. Mol. Sci.* 21.
- Taurin, S., Alkhalifa, H., 2020. Breast cancers, mammary stem cells, and cancer stem cells, characteristics, and hypotheses. *Neoplasia* 22, 663–678.
- Tavares, S., et al., 2017. Actin stress fiber organization promotes cell stiffening and proliferation of pre-invasive breast cancer cells. *Nat. Commun.* 8, 15237.
- Tiwari, N., et al., 2013. Klf4 is a transcriptional regulator of genes critical for EMT, including Jnk1 (Mapk8). *PLoS One* 8, e57329.
- Tomitsch, J., Dechant, E., 2015. Exposure to electromagnetic fields in households—trends from 2006 to 2012. *Bioelectromagnetics* 36, 77–85.
- Tyanova, S., et al., 2016. The Perseus computational platform for comprehensive analysis of (prote)omic data. *Nat. Methods* 13, 731–740.
- Tyanova, S., Cox, J., 2018. Perseus: A Bioinformatics Platform for Integrative Analysis of Proteomics Data in Cancer Research. *Methods Mol. Biol.* 1711, 133–148.
- Valberg, P.A., et al., 1997. Can low-level 50/60 Hz electric and magnetic fields cause biological effects? *Radiat. Res* 148, 2–21.
- Wang, M.H., et al., 2021. Effect of extremely low frequency electromagnetic field parameters on the proliferation of human breast cancer. *Electro Biol. Med* 40, 384–392.
- Wang, Y., et al., 2019. Exposure to a 50Hz magnetic field at 100 μ T exerts no DNA damage in cardiomyocytes. *Biol. Open* 8.
- Wertheimer, N., Leeper, E., 1979. Electrical wiring configurations and childhood cancer. *Am. J. Epidemiol.* 109, 273–284.
- Wolf, F.I., et al., 2005. 50-Hz extremely low frequency electromagnetic fields enhance cell proliferation and DNA damage: possible involvement of a redox mechanism. *Biochim Biophys. Acta* 1743, 120–129.
- Wu, H.J., et al., 2020. FAK signaling in cancer-associated fibroblasts promotes breast cancer cell migration and metastasis by exosomal miRNAs-mediated intercellular communication. *Oncogene* 39, 2539–2549.
- Xu, A., et al., 2020. Low-frequency magnetic fields (LF-MFs) inhibit proliferation by triggering apoptosis and altering cell cycle distribution in breast cancer cells. *Int J. Mol. Sci.* 21.
- Zhang, D., et al., 2017. Resveratrol may reverse the effects of long-term occupational exposure to electromagnetic fields on workers of a power plant. *Oncotarget* 8, 47497–47506.
- Zhang, Q., et al., 2019. Identification of potential diagnostic and prognostic biomarkers for prostate cancer. *Oncol. Lett.* 18, 4237–4245.
- Zhang, Y., et al., 2016. Meta-analysis of extremely low frequency electromagnetic fields and cancer risk: a pooled analysis of epidemiologic studies. *Environ. Int* 88, 36–43.
- Zhang, Y., et al., 2018. Extremely low frequency electromagnetic fields promote mesenchymal stem cell migration by increasing intracellular Ca²⁺ and activating the FAK/Rho GTPases signaling pathways in vitro. *Stem Cell Res Ther.* 9, 143.